J Mol Model (2012) 18:3061–3072
DOI 10.1007/s00894-011-1317-8

ORIGINAL PAPER

Density functional study on size-dependent structures, stabilities, electronic and magnetic properties of Au_nM (M = Al and Si, n=1–9) clusters: comparison with pure gold clusters

Yan-Fang Li · Ai-Jie Mao · Yang Li · Xiao-Yu Kuang

Received: 8 September 2011 / Accepted: 21 November 2011 / Published online: 14 December 2011

Abstract The density functional theory (DFT) method has been employed to systematically investigate the geometrical structures, relative stabilities, and electronic and magnetic properties of Au_nM (M = Al and Si, n=1–9) clusters for clarifying the effect of Al (Si) modulation on the gold nanostructures. Of all the clusters studied, the most stable configurations adopt a three-dimensional structure for Au_nAl at n=4–8 and Au_nSi at n=3–9, while for pure gold systems, no three-dimensional lowest energy structures are obtained. Through a careful analysis of the fragmentation energy, second-order difference of energy, HOMO-LUMO energy gap, and magnetic moment as a function of cluster size, an odd-even alternative phenomenon has been observed. The results show that the clusters with even-number valence electrons have a higher relative stability, but lower magnetic moments. Furthermore, Al (Si) doping is found to enhance the stabilities of gold frameworks. In addition, the charge analysis has been given to understand the different effects of individual doped atom on electronic properties and compared further.

Keywords Cluster · Density functional theory · Electronic property · Geometric configuration · Relative stability

Electronic supplementary material The online version of this article (doi:10.1007/s00894-011-1317-8) contains supplementary material, which is available to authorized users.

Y.-F. Li · A.-J. Mao (✉) · X.-Y. Kuang
Institute of Atomic and Molecular Physics, Sichuan University, Chengdu 610065, China
e-mail: scu_kuang@163.com

X.-Y. Kuang
International Centre for Materials Physics, Academia Sinica, Shenyang 110016, China

Y. Li
Department of Opto-Electronics Science and Technology, Sichuan University, Chengdu 610065, China

Introduction

As a bridge between molecular state and alloy condensed matter, cluster researches have been expanded into abundant aspects of solid state physics, atomic and molecular physics, and physical chemistry [1–5]. This is because of the motivations for designing new types of nanofunctional materials with unique optical, magnetic, microelectronic, medicinal, nanotechnologic, and thermal properties.

Since the closed subshell and limited number of valence electrons can greatly simplify theoretical simulation and spectroscopic measure, during the last decade, investigations of alkali metal series and coinage metal clusters have been an active field to understand the structural and physicochemical properties in depth [6–10]. Among them, the structures of small lithium cluster anions have been determined by a combination of anion photoelectron spectroscopy and ab initio calculation [11]. Alexandrova et al. predicted that the planar geometries are energetically preferred up to n=4 for Li_n^-. For coinage metal clusters, numerous theoretical works performed by different programs [12–18], such as Siesta, Gaussian, DMOL, VASP, etc., have demonstrated that gold clusters are more in favor of 1D and 2D conformations than silver and copper due to a strong *sd* hybridization in Au. Meanwhile, a pronounced catalytic activity related to gold nanoparticles containing as few as 7–8 atoms is also noticeable [8, 19].

In comparison to pure gold clusters, it is well known that the properties of clusters can be profoundly influenced by the presence of impurities, so doping of gold clusters with

different atoms has been expected to open up possible routes to clarify bonding characteristics between consistent atoms [20–24]. The effects of isoelectronic substitution on the electronic and structural properties of gold cluster anions: Au_nM^- (M = Ag, Cu, n=8–11) have been investigated in the critical size range of the 2D → 3D structural transition by Wang et al. [25]. Photoelectron spectra indicate that substitution of an Au atom by a single Ag or Cu atom does not significantly affect the geometrical and electronic structures of the clusters, and $Au_{11}M^-$ is found to be the critical size due to only 3D isomers being observed. To provide further insight on Au-Cu system, recently, we have studied the doping of the small neutral, anionic, and cationic gold clusters by impurity atom, bimetallic $Au_nCu^{0,\pm1}$ (n=1–8) [26]. The most stable structures of neutral and anionic systems have a planar structure and resemble pure gold clusters in shape, whereas the geometries of Au_nCu^+ undergo a structural change when n=6. At the same time, Yuan et al. [27] have found that in the Pt-group doped gold clusters Au_nM (M = Ni, Pd, Pt, n=1–7) the doped atoms markedly change the geometrical, electronic, and bonding properties of gold cluster; also, the element- and size-dependent electron stabilities and delocalization as well as magnetic properties of Au_nM^+ (M = Sc, Ti, V, Cr, Mn, Fe, $n \leq 9$) and Au_nM^+ (M = Sc, Ti, V, Cr, Mn, Fe, Co, Ni, $n \leq 40$) clusters, respectively, have been reported by Torres and Neukermans et al. [28, 29]. One can find that the properties of clusters vary sensitively with their sizes and compositions and differ from those in bulk. In contrast to that mentioned above, it may be noted that more and more attention has been focused on group-III elements since they contribute only *s-p* states to the valence band, in this way, they are prototype materials to examine the effects of *spd* hybridization and understand their potential technological applications in microelectronics [30–36]. Based on DFT, Majumder et al. [37] have calculated the geometrical and electronic structures of Na, Mg, Al, Si, P, S doped in Au_6 clusters, interesting, whose results show that impurities with *p* electrons (Al, Si, P) yield nonplanar Au_5M clusters, while those with *s* electrons (Na, Mg) yield planar geometries. Although the intermetallic clusters Au_nNa and Au_nMg^{-1} have been studied [38, 39], the open phenomenon remains in question: whether the phenomenon observed in [37] can be found in the other cluster sizes? If so, how does the composition of dopant affect the growth pattern? Furthermore, are their structures and properties greatly distinct from the pure gold clusters?

In order to explore further insight on gold-containing clusters, in this paper, we investigate the evolutions of geometries, stabilities, electronic and magnetic properties of Au_nM (M = Al and Si, n=1–9) clusters by using the first-principle method based on DFT, and combined with pure gold ones for comparison. The calculated fragmentation energies, second-order difference of energies, HOMO-LUMO energy gaps, and magnetic moments show a similar odd-even alternative behavior with the cluster size. In addition, it is found that the properties of both clusters are related to a strong *s-p* orbital interaction. In the following section, we briefly outline the computational methodology. In Results and discussion, the results are presented and discussed, which are then summarized in Conclusions.

Theoretical methods and computational details

The lowest energy configurations and the other low-lying isomers for both Au_nAl and Au_nSi (n=1–9) clusters are investigated by means of *GAUSSIAN 03* program package with a gradient-corrected exchange and correlation functional *Perdew-Wang* (PW91) [40, 41]. For Au atoms, a full electron calculation is rather time consuming, therefore it is better to introduce the relativistic effective core potential (RECP) Stuttgart/Dresden double-zeta SDD basis set [42, 43], which is adopted to describe the $5s^25p^65d^{10}6s^1$ outermost valence electrons. Meanwhile, Wachter-Hay all electron basis set 6–311 G* is used for the doped atoms Al and Si. In this connection, the basis set labeled GEN is a combination of 6–311 G* basis set for dopants and SDD basis set for Au atoms. In searching for the lowest energy structures, lots of possible initial configurations, including 1D, 2D, or 3D structures, have been extensively explored without any symmetry constraint, and different spin multiplicities are also taken into account by considering the spin polarization in geometry optimizations. In the optimizing process, the structures are regarded as optimized when the convergence thresholds of the maximum force, root-mean-square (RMS) force, maximum displacement of atoms, and RMS displacement of atoms are set to 0.00045, 0.0003, 0.0018, and 0.0012 au, respectively. Furthermore, for each stationary point of cluster, the stability is examined by performing a vibrational frequency calculation. In case an imaginary frequency is found, a relaxation along the coordinates of the imaginary vibrational mode is carried out until the true local minimum is actually obtained. In this way, for each cluster size, a large number of stable isomers are obtained, but here we only report a few energetically low-lying ones. It should be pointed out that, in order to comparatively study the properties of different impurities doped in gold clusters, some similar low-lying isomers are selected for Au_nAl and Au_nSi systems in our discussions.

Here, a testing calculation has been performed with the purpose of checking the validity of computational method. The biatomic AuAl cluster with $^1\sum$ electronic state is the ground-state structure. Its equilibrium bond length is 2.39 Å, which overestimates the measured value 2.34 Å. However, the calculated vibrational frequency 318 cm^{-1} and dissociation energy 3.48 eV fall close to experimental results of

330 cm^{-1} and 3.37 ± 0.13 eV [44, 45]. For AuSi, its theoretical results of bond length 2.28 Å and dissociation energy 3.17 eV are in good agreement with available experimental data 2.26 Å [46] and 3.16 eV [47]. This result excels that of hybrid exchange-correlation functional B3LYP (2.41 Å and 3.12 eV for AuAl, 2.30 Å and 2.73 eV for AuSi), thus, in the present work, we can use the chosen computational method to describe small Au_nM (M = Al and Si) clusters.

Results and discussion

The ground-state structures and a number of optimized low-energy configurations for Au_nM (M = Al and Si, n=1–9) clusters are shown in Figs. 1 and 2, respectively, which are designated by na, nb, nc, nd, and ne (n is the number of Au atoms in Au_nM clusters) according to the total energy from low to high. Meanwhile, the corresponding electronic states, symmetries, total energies, as well as relative energies are summarized in Table 1. In order to investigate the effects of doping impurity, such as Al or Si, on gold clusters, optimizations are also performed for Au_{n+1} (n=1–9) clusters by using PW91/SDD method. Although many possible initial structures have been taken into account, only the most stable geometry for each size are shown in Fig. 1. All the gold clusters are found to prefer the lowest spin state, and no 3D structures are observed up to Au_{10}, which is in line with the previous DFT calculations [14, 15]. In this section, first, we will discuss the general features observed in Au_nM clusters and compare the results with homoatomic Au_{n+1} clusters.

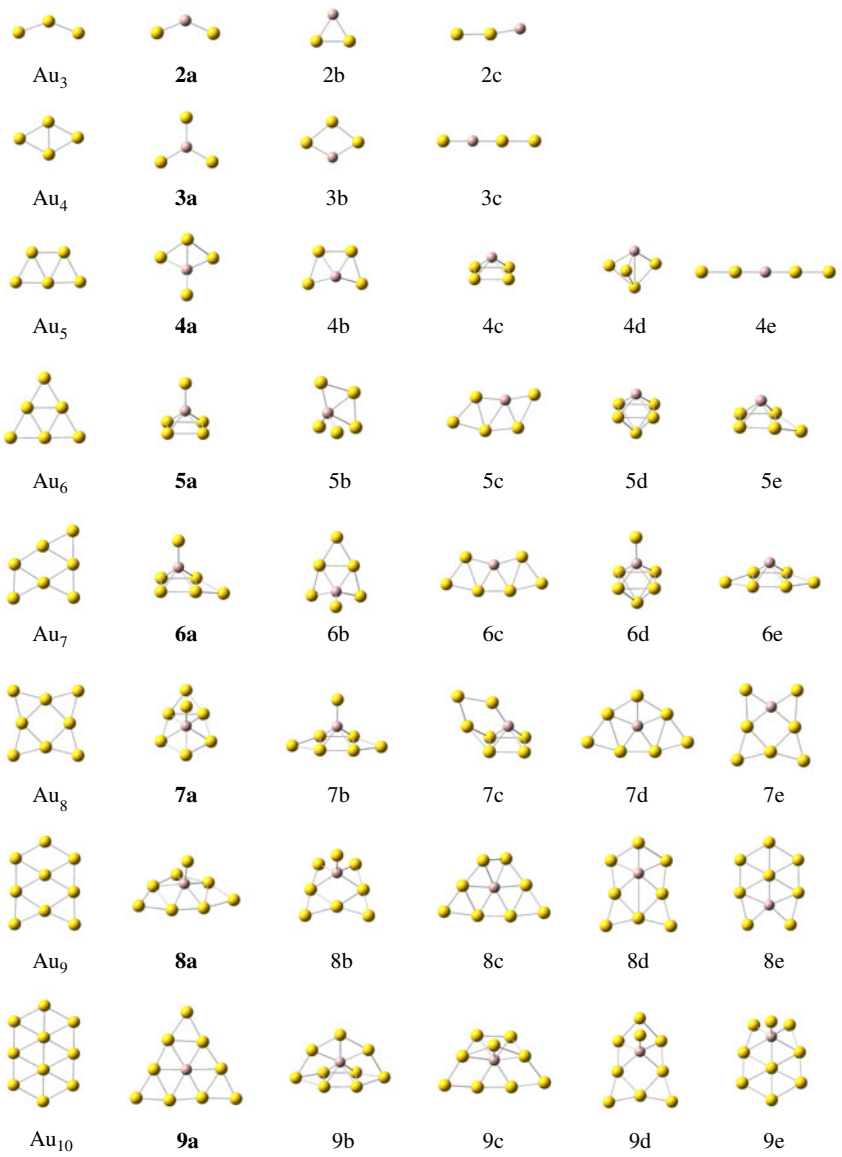

Fig. 1 The lowest energy structures and low-lying isomers for Au_nAl (n=1–9) clusters at the PW91/GEN (6–311 G* for dopants and SDD for Au) level, and the ground-state structures of pure gold clusters Au_{n+1} (n=1–9) have been listed on the left. The lowest energy isomers are denoted in bold

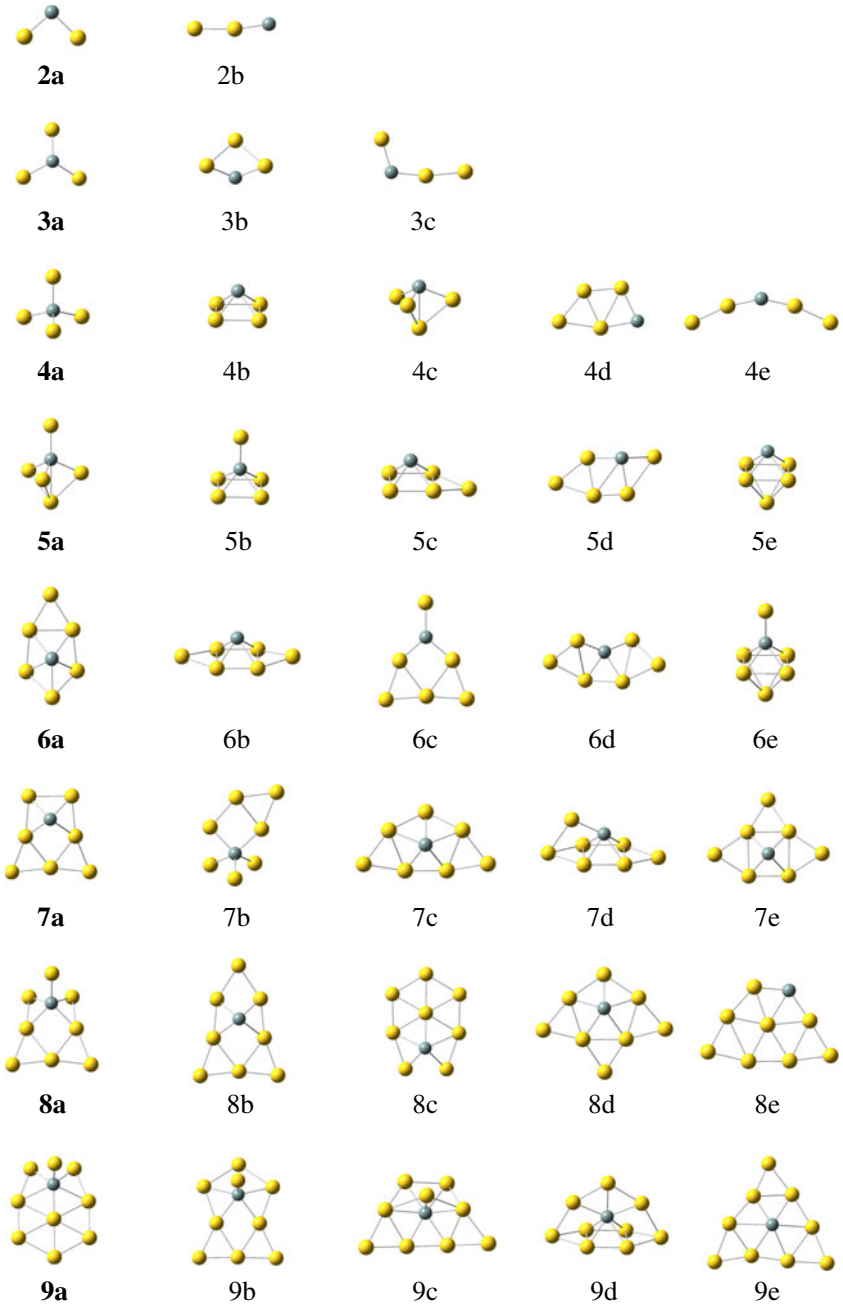

Fig. 2 The lowest energy structures and low-lying isomers for Au_nSi (n=1–9) clusters at the PW91/GEN (6–311 G* for dopants and SDD for Au) level. The lowest energy isomers are denoted in bold

Equilibrium geometry

The most stable structure of Au_2Al cluster is similar to the corresponding pure Au_3 cluster with the Al atom at the middle, in which Au-Al bond lengths and Au-Al-Au apex angle are 2.37 Å and 131.5°, respectively. The C_{2v} isosceles triangle (63.2°) 2b and distorted linear structure 2c are low-lying isomers and higher in energy than that of isomer 2a by 0.43 and 0.88 eV. Addition of one Au atom to Au_2Al (2a) leads to a high-symmetry planar structure 3a with the lowest energy. In this structure, the aluminum atom occupies a center position of a Au_3 equilateral triangle, so it possesses three equal Au-Al bonds (2.36 Å). Our calculations reveal that the planar rhombus is the ground-state configuration of Au_4 cluster. However, the rhombus Au_3Al cluster is 0.67 eV energetically higher than 3a. Starting from n=4, the five-atoms system Au_4Al is the smallest cluster to show appearance of 3D structural isomer, which can be obtained by adding an Au atom to rhombus 3b. The other three Au_4Al isomers, trapezia-shaped structure (4b), square pyramid structure (4c), and triangular bipyramid structure (4 d), also have 3D geometries which are, respectively, 0.28, 0.30, and 0.56 eV above the lowest energy structure. For isomer 4c, it has a high geometrical symmetry C_{4v}, whereas it is not the ground-state Au_4Al cluster in our optimized results.

Table 1 Electronic states, symmetries, total energies (E_T), and relative energies (ΔE) for Au_nM (M = Al and Si, n=1–9) clusters at the PW91/GEN (6–311 G* for dopants and SDD for Au) level. The lowest energy isomers are denoted in bold

Cluster	Is.	State	Sym.	E_T (au)	ΔE (eV)	Cluster	Is.	State	Sym.	E_T (au)	ΔE (eV)
Au_2Al	**2a**	$^2A_1$	C_{2v}	**−514.15206**	**0.00**	Au_2Si	**2a**	$^1A_1$	C_{2v}	**−561.19210**	**0.00**
	2b	$^2B_2$	C_{2v}	−514.13610	0.43		2b	$^1A'$	C_s	−561.13248	1.62
	2c	$^2A'$	C_s	−514.11982	0.88						
Au_3Al	**3a**	$^1A_1$	D_{3h}	**−650.06255**	**0.00**	Au_3Si	**3a**	$^2A_1$	C_{3v}	**−697.07211**	**0.00**
	3b	$^1A_1$	C_{2v}	−650.03805	0.67		3b	$^2A'$	C_s	−697.06497	0.19
	3c	$^1\sum$	$C_{\infty v}$	−650.03313	0.80		3c	$^2A'$	C_s	−697.03781	0.93
Au_4Al	**4a**	$^2A'$	C_s	**−785.92131**	**0.00**	Au_4Si	**4a**	$^1A_1$	D_{2d}	**−832.97577**	**0.00**
	4b	$^2A'$	C_s	−785.91093	0.28		4b	$^1A_1$	C_{4v}	−832.96781	0.22
	4c	$^2A_1$	C_{4v}	−785.91028	0.30		4c	$^1A_1$	C_{3v}	−832.96774	0.22
	4d	$^2A''$	C_s	−785.90060	0.56		4d	$^1A'$	C_s	−832.92587	1.36
	4e	$^2\sum_u$	$D_{\infty h}$	−785.88136	1.09		4e	$^1A_1$	C_{2v}	−832.90594	1.90
Au_5Al	**5a**	$^1A_1$	C_{4v}	**−921.82290**	**0.00**	Au_5Si	**5a**	$^2A_1$	C_{3v}	**−968.82978**	**0.00**
	5b	$^1A'$	C_s	−921.81656	0.17		5b	$^2A_1$	C_{4v}	−968.82871	0.03
	5c	$^1A'$	C_s	−921.80898	0.38		5c	$^2A'$	C_s	−968.82611	0.10
	5d	$^1A_1$	C_{4v}	−921.80185	0.57		5 d	$^2A_1$	C_{4v}	−968.81418	0.42
	5e	$^1A'$	C_s	−921.79243	0.83		5e	$^2A''$	C_s	−968.79310	1.00
Au_6Al	**6a**	$^2A'$	C_s	**−1057.68520**	**0.00**	Au_6Si	**6a**	$^1A'$	C_s	**−1104.72172**	**0.00**
	6b	$^2A'$	C_s	−1057.68347	0.05		6b	$^1A_1$	C_{2v}	−1104.71864	0.08
	6c	$^2B_2$	C_{2v}	−1057.68049	0.13		6c	$^1A_1$	C_{2v}	−1104.71387	0.21
	6d	$^2A_1$	C_{4v}	−1057.68007	0.14		6d	^1A	C_2	−1104.70805	0.38
	6e	$^2A_1$	C_{2v}	−1057.67424	0.30		6e	$^1A_1$	C_{4v}	−1104.70681	0.41
Au_7Al	**7a**	$^1A'$	C_s	**−1193.58571**	**0.00**	Au_7Si	**7a**	$^2A'$	C_s	**−1240.59665**	**0.00**
	7b	$^1A_1$	C_{2v}	−1193.58557	0.00		7b	^2A	C_1	−1240.59096	0.15
	7c	$^1A'$	C_s	−1193.58035	0.15		7c	$^2A''$	C_s	−1240.58932	0.20
	7d	$^1A_1$	C_{2v}	−1193.57782	0.21		7d	$^2A'$	C_s	−1240.58664	0.27
	7e	$^1A_1$	C_{2v}	−1193.56913	0.45		7e	$^2A'$	C_s	−1240.58143	0.41
Au_8Al	**8a**	$^2A''$	C_s	**−1329.46326**	**0.00**	Au_8Si	**8a**	$^1A'$	C_s	**−1376.49849**	**0.00**
	8b	$^2A'$	C_s	−1329.45831	0.13		8b	$^1A'$	C_s	−1376.48902	0.26
	8c	^2A	C_2	−1329.45627	0.19		8c	$^1A'$	C_s	−1376.48643	0.33
	8d	$^2A'$	C_s	−1329.45402	0.25		8d	$^1A'$	C_s	−1376.46624	0.88
	8e	$^2A'$	C_s	−1329.45360	0.26		8e	$^1A'$	C_s	−1376.46513	0.91
Au_9Al	**9a**	$^1A'$	C_{3h}	**−1465.36262**	**0.00**	Au_9Si	**9a**	$^2A'$	C_s	**−1512.36607**	**0.00**
	9b	$^1A_1$	C_{2v}	−1465.36239	0.01		9b	$^2A'$	C_s	−1512.36113	0.13
	9c	^1A	C_1	−1456.35992	0.07		9c	^2A	C_1	−1512.35298	0.36
	9d	$^1A'$	C_s	−1465.35713	0.15		9d	$^2A_1$	C_{2v}	−1512.35284	0.36
	9e	$^1A'$	C_s	−1465.35423	0.23		9e	^2A	C_1	−1512.34991	0.44

When one, two, or three gold atoms are added to the different locations of isomer 4c, the other 3D structures (5a, 5d, 5e, 6a, 6d, 6e, 7b, 7c) are optimized, respectively. Meanwhile, in these eight configurations, the geometrical symmetries are C_{4v} for 5a, 5 d, and 6 d, C_{2v} for 6e and 7b, as well as C_s for 5e, 6a, and 7c. From n=7, it can be seen that the Al atom gets inside in the gold framework. The most stable isomer 7a is obtained by adding Au atom to 6b isomer while the least stable isomer 7e is formed by substituting one gold atom of ground-state Au_8 cluster by impurity. After an Au atom is capped on the triangle structure 7 d in 2.36 Å, the lowest energy structure 8a, which remains a 3D geometry, is generated. Among these Au_8Al clusters, the 3D isomers 8d and 8e with C_s symmetry and $^2A'$ electronic state can be viewed as a substituted structure of Au_9, in which the aluminum atom locates in different positions. Therefore, their relative energies are almost degenerate, that is, 0.25 and 0.26 eV. When the number of Au_nAl clusters is increased to ten, surprisingly, we find a planar triangle configuration 9a to be the ground-state structure, which is different from the conclusion of Zhao [48]. Again we performed an

extensive search for other isomers. In our subsequent search for the local minimum, we find a 3D boat-shaped structure 9b to be also lowest in energy and almost degenerate with isomer 9a (0.01 eV). This energy difference is clearly smaller than the error inherent in the computational method. As for the other three low-lying isomers 9c, 9d, and 9e, they are optimized in the energy range 0.23 eV.

Now we present the geometrical features of Au_nSi clusters, whose equilibrium structures of the most stable configurations and the low-lying isomers are shown in Fig. 2. As a general trend, it is obtained that the ground-state Au_nSi clusters adopt a 3D structure with the lowest spin multiplicity for $3 \leq n \leq 9$, and all of them are different from the corresponding pure Au_{n+1} clusters. That is to say the doping of one silicon atom in Au_{n+1} clusters can obviously change the geometry of the pure gold framework. By comparing Figs. 1 and 2, meanwhile, we can find that although the low-energy structures of Au_nAl and Au_nSi are somewhat similar for most of the sizes, the order of these isomers is reversed. Moreover, in the case of Au_nSi, with a few exceptions, the structures transfer from 2D to 3D more easily. For examples, the capped-triangle structure 3a, rhombus structure 3b, distorted parallelogram structure 5d, trapezoidal structure 6d, triangle structure 7c and 9e are 3D, while those of Au_nAl are planar. The most stable Au_2Si is an obtuse triangle (2a) and a distorted linear structure (2b) is a low-lying one. The optimized Au-Si bond lengths of 2a and 2b are found to be 2.30 and 2.24 Å, respectively, and the apex angle of 2a is 93.3°, which are smaller than those of Au_2Al. Comparing with the least stable linear structure of Au_3Al, a similar calculated result has been obtained in silicon, whereas the geometry of 3c is distorted due to the effect of Si atom. Also, on the basis of square pyramid Au_4Si cluster 4b, seven derived structures (5b, 5c, 5e, 6b, 6e, 7d, and 7e) are obtained when Au atoms are added on different sites of it. Similarly, the ground-state Au_5Si 5a are optimized and guided by the stable isomer 4c. This triangular pyramid with C_{3v} symmetry first appears, whose total energy is only 0.03 eV lower than the next stable isomer, Au-capped square pyramid. Recently, Majumder et al. [37] have shown that when Au clusters interact with impurity elements possessing *p* electrons, a preference of 3D structural transition occurs due to the sp^3 hybridization. Using this information as a guide, the calculation again predicts 3D structures to be the lowest in energy from n=6 to n=9; interestingly, the most stable isomers of Au_6Si and Au_7Si can be described as one and two gold atoms being added to 5c geometry, respectively, while the 8a isomer is found by top-capping the Au atom onto generated structure 7a. With regard to Au_8Si, the nonplanar isomer 8b is consistent with the prediction of Majumder by using the program VASP, [18] but this structure is 0.26 eV higher in total energy than the ground state 8a in our calculated result.

From the above discussion, it can be noted that the lowest energy structures of Au_nAl clusters for n=4–8 and Au_nSi clusters for n=3–9 favor a 3D geometry. Although Au_9Al has a planar structure, it is almost energetically degenerate with a 3D isomer. In contrast to this, the conclusion is widely different from the phenomenon observed in pure gold clusters and the other previous studies on transition-metal or group-III-element Na, Mg doped gold clusters. This indicates that doping with a single Al or Si atom dramatically affects the geometries of the ground-state Au_{n+1} clusters. Considering the growth patterns, impurity substituted Au_{n+1} clusters and Au atoms added Au_{n-1} M (M = Al and Si, n=1–9) structures for different Au_nM clusters are dominant.

Size dependence of relative stability

In cluster physics, the atomic average binding energy E_b, fragmentation energy Δ_1E, and second-order difference of energy Δ_2E have proved to be a powerful tool to reflect the relative stabilities of the clusters. In order to analyze the stability and size-dependent properties of Au_nM (M = Al and Si, n=1–9) clusters, based on the lowest energy structures, we calculate the corresponding E_b, Δ_1E (with respect to removing one Au atom from cluster), and Δ_2E, which are defined as the following formulas:

$$\begin{aligned} E_b(n) &= [nE(\mathrm{Au}) + E(\mathrm{M}) - E(\mathrm{Au}_n\mathrm{M})]/(n+1) \\ \Delta_1E(n) &= E(\mathrm{Au}_{n-1}\mathrm{M}) + E(\mathrm{Au}) - E(\mathrm{Au}_n\mathrm{M}) \\ \Delta_2E(n) &= E(\mathrm{Au}_{n-1}\mathrm{M}) + E(\mathrm{Au}_{n+1}\mathrm{M}) - 2E(\mathrm{Au}_n\mathrm{M}) \end{aligned} \quad , \quad (1)$$

where n is the number of gold atoms in the Au_nM (M = Al and Si) clusters and E (Au), E (M), E (Au_nM), E (Au_{n-1} M), and E (Au_{n+1} M) represent the total energies of the ground-state atoms or clusters for Au, Al (Si), Au_nM, Au_{n-1} M, and Au_{n+1} M, respectively. Considering the influence of the impurity atoms on small pure framework, the atomic average binding energy E_b, fragmentation energy Δ_1E (with respect to removing one Au atom from cluster), and second-order difference of energy Δ_2E of Au_{n+1} clusters are also studied, which are expressed as:

$$\begin{aligned} E_b(n+1) &= [(n+1)E(\mathrm{Au}) - E(\mathrm{Au}_{n+1})]/(n+1) \\ \Delta_1E(n+1) &= E(\mathrm{Au}_n) + E(\mathrm{Au}) - E(\mathrm{Au}_{n+1}) \\ \Delta_2E(n+1) &= E(\mathrm{Au}_n) + E(\mathrm{Au}_{n+2}) - 2E(\mathrm{Au}_{n+1}) \end{aligned} \quad , \quad (2)$$

where E(Au), E(Au_{n+1}), E(Au_n), and E(Au_{n+2}) remain the total energies of ground-state atoms or clusters.

Based on the above formulas, the calculated results of atomic average binding energies, fragmentation energies (with respect to removing one Au atom from cluster), and second-order difference of energies are obtained, which are summarized in Table 2, and Fig. 3a, b as well as c, respectively, describe their dependences with respect to cluster size. As for the atomic average binding energies, the

primary features are concluded: (i) For pure gold clusters, Fig. 3a illustrates that the E_b has an increasing tendency with the cluster size growing. This reflects the fact that the bigger the clusters, the more stable the molecular properties, which agrees with the previous work. (ii) For Au_nAl, the E_b increases continuously to a maximum when the size increases from n=1 to n=3; then, a slight odd-even effect arises for $n > 3$ which shows a higher stability of odd-numbered clusters than even-numbered sizes. Therefore, a visible peak occurs at n=3, indicating that the Au_3Al cluster is relatively more stable in the region of n=1–9. A similar alternation is also found for Au-Si system, and there are two local peaks corresponding to Au_2Si and Au_4Si clusters. (iii) Meanwhile, as presented in Fig. 3a, the E_b values of Au_nM (M = Al and Si) clusters are significantly higher than those of Au_{n+1} clusters, hinting that the impurities Al and Si can improve the stabilities of gold clusters.

In view of the fragmentation energies with respect to single Au dissociation and second-order difference of energies, they are quite sensitive quantities that reflect the relative stability of cluster. For Au_nM (M = Al and Si) and Au_{n+1} clusters, both Fig. 3b and c show that the cluster stabilities exhibit pronounced odd-even alternations as a function of cluster size. It indicates that the pure and Al-doped clusters, at n=3, 5, 7, and 9, while Si-doped clusters, at n=2, 4, 6, and 8, have a higher relative stability than their neighbors. However, the doping Si atom makes the stable pattern of host clusters contrary, which may be caused by a paired p valence electron in silicon atom. Whether the outmost valence electrons paired or unpaired, both pure and doped gold clusters with even-number valence electrons are more stable than those with odd-number valence electrons. In particular, the most stable structures can be assigned to 6-electron systems for Au_nAl and Au_{n+1} clusters since the calculated highest values of Δ_1E (2.95 eV for Au_3Al and 2.98 eV for Au_6) and Δ_2E (1.41 eV for Au_3Al and 1.45 eV for Au_6), which is consistent with the observation in the atomic average binding energies. With regard to Au_nSi clusters, although we can find a maximal intensity at n=2 (3.15 eV) for the fragmentation energies, followed by the Au_4Si cluster, whereas the curve of second-order difference of energies shows a prominent peak at n=4 (1.35 eV).

Next, in order to investigate further the relative stability preferred by a cluster, we present the fragmentation channel involving an impurity atom, that is, $\Delta_1E = E(Au_n) + E(M) - E(Au_nM)$. Considering the dependence of the Δ_1E (M dissociation) on the cluster size, the relationships of Δ_1E versus n are plotted in Fig. 3d. For Au_nAl (n=1–9) clusters, a pronounced odd-even oscillation also can be depicted from the curve. It confirms a higher relative stability of Au_nAl clusters at n=3, 5, 7, and 9. Different from aluminum, the fragmentation energies of Au-Si series sharply reach maximum at Au_4Si and decrease dramatically for n=4–6. As a consequence, the maximum values at n=3 (5.08 eV) and n=4 (5.37 eV) are found for Au_3Al and Au_4Si clusters, respectively, suggesting they keep the highest stability. In addition, the positive values of Δ_1E mean that the dissociation of one atom is an unfavorable process. Therefore, if Δ_1E (Au) > Δ_1E (M), the impurity dissociation is favorable; on the contrary, Δ_1E (Au) < Δ_1E (M) corresponds to a preferred Au dissociation. In Table 2, it is easy to see that the dissociation of Au is favored for both series Au_nAl and Au_nSi at n=1–9. Hence, it can be predicted that the addition of Al and Si to an Au_n cluster is energetically favorable.

Electronic properties

The highest occupied-lowest unoccupied molecular orbital (HOMO-LUMO) energy gap reflects the ability of an electron to jump from occupied orbital to unoccupied orbital, in a sense, it can provide an important criterion to study the chemical stability of a cluster. For the lowest energy structures of Au_nM (M = Al and Si, n=1–9) clusters, compared with bare gold series, the trends of HOMO-LUMO energy

Table 2 Atomic average binding energy (E_b), fragmentation energy (Δ_1E), and second-order difference of energy (Δ_2E) for the lowest energy Au_nM (M = Al and Si, n=1–9) and Au_{n+1} clusters at the PW91/GEN (6–311 G* for dopants and SDD for Au) level

Property	Cluster	n=1	n=2	n=3	n=4	n=5	n=6	n=7	n=8	n=9
E_b (eV)	Au_nAl	1.75	1.85	2.13	2.01	2.13	2.06	2.13	2.13	2.18
	Au_nSi	1.59	2.11	2.11	2.24	2.10	2.15	2.13	2.20	2.15
	Au_{n+1}	1.10	1.14	1.46	1.60	1.83	1.78	1.90	1.89	1.97
Δ_1E-Au (eV)	Au_nAl	–	2.05	2.95	1.54	2.71	1.64	2.68	2.05	2.65
	Au_nSi	–	3.15	2.12	2.76	1.41	2.45	1.98	2.71	1.78
	Au_{n+1}	–	1.23	2.40	2.15	2.98	1.53	2.73	1.79	2.73
Δ_1E-M (eV)	Au_nAl	3.51	3.36	5.08	4.22	4.77	3.43	4.58	3.90	4.76
	Au_nSi	3.17	4.13	5.01	5.37	4.64	4.10	4.55	4.54	4.53
Δ_2E (eV)	Au_nAl	–	−0.90	1.41	−1.17	1.07	−1.04	0.63	−0.59	–
	Au_nSi	–	1.03	−0.64	1.35	−1.03	0.46	−0.73	0.93	–
	Au_{n+1}	–	−1.17	0.25	−0.83	1.45	−1.20	0.94	−0.94	–

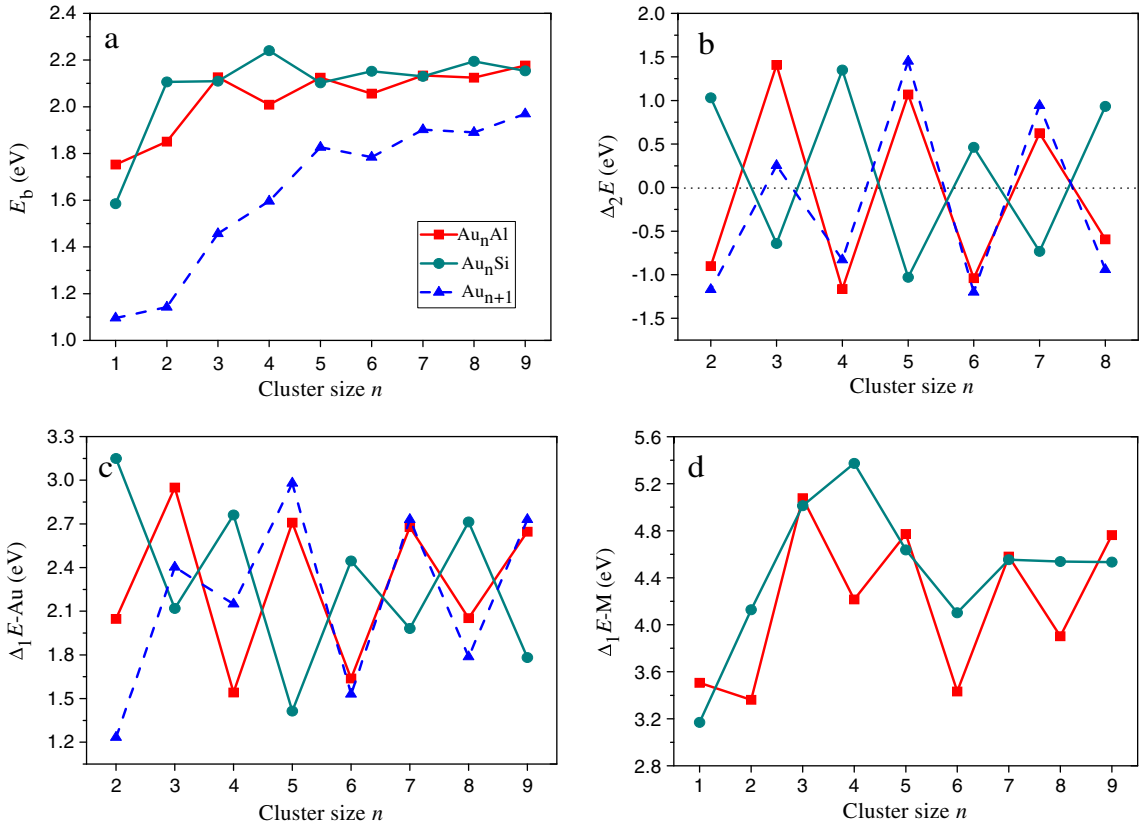

Fig. 3 Size dependences of (**a**) the atomic average binding energies, (**b**) the second-order difference of energies, (**c**) the fragmentation energies with respect to removing one Au atom from cluster, and (**d**) the fragmentation energies with respect to removing M atom from cluster for Au_nM (M = Al and Si) and Au_{n+1} clusters in the size range n=1–9 at the PW91/GEN (6–311 G* for dopants and SDD for Au) level

gaps with respect to cluster size are plotted in Fig. 4. It can be seen that the HOMO-LUMO energy gaps of Au_nM (M = Al and Si) and Au_{n+1} clusters present a similar odd-even oscillatory behavior as observed in the fragmentation energies (with respect to removing one Au atom from cluster) and second-order difference of energies. Namely, the clusters with even-number valence electrons have large HOMO-LUMO energy gaps and are relatively weaker in chemical activity than those with odd-number valence electrons. As seen in molecular orbital energy levels (Fig. 5 and Supporting Information), the enhanced chemical stabilities can be explained by the electron paired effect. The $Au_{1,3,5,7,9}Al$, $Au_{2,4,6,8}Si$, and $Au_{2,4,6,8,10}$ clusters have even-number valence electrons and their HOMOs are doubly occupied. The electrons in a doubly occupied HOMO have a stronger effective core potential because of the electron screening being weaker for electrons in the same orbital than for inner shell electrons. Thus, the LUMO can hardly acquire an electron from the closed-shell HOMO of an even-number system than in the open-shell systems. In this way, the clusters with even number of valence electrons are relatively stable. Besides, it is worth pointing out that the largest HOMO-LUMO energy gaps of 2.49, 2.06, and 2.16

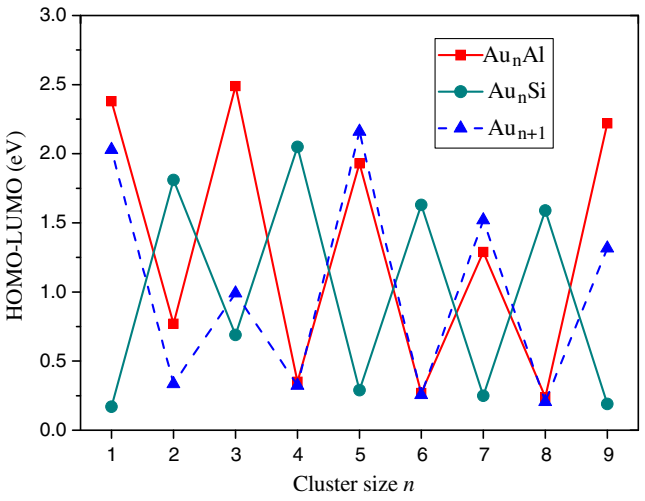

Fig. 4 Size dependence of the HOMO-LUMO energy gaps for the lowest energy Au_nM (M = Al and Si, n=1–9) and Au_{n+1} clusters at the PW91/GEN (6–311 G* for dopants and SDD for Au) level

Fig. 5 Molecular orbital energy levels for the lowest energy structures of Au_nAl (n=1–9) clusters at the PW91/GEN (6–311 G* for dopants and SDD for Au) level ▶

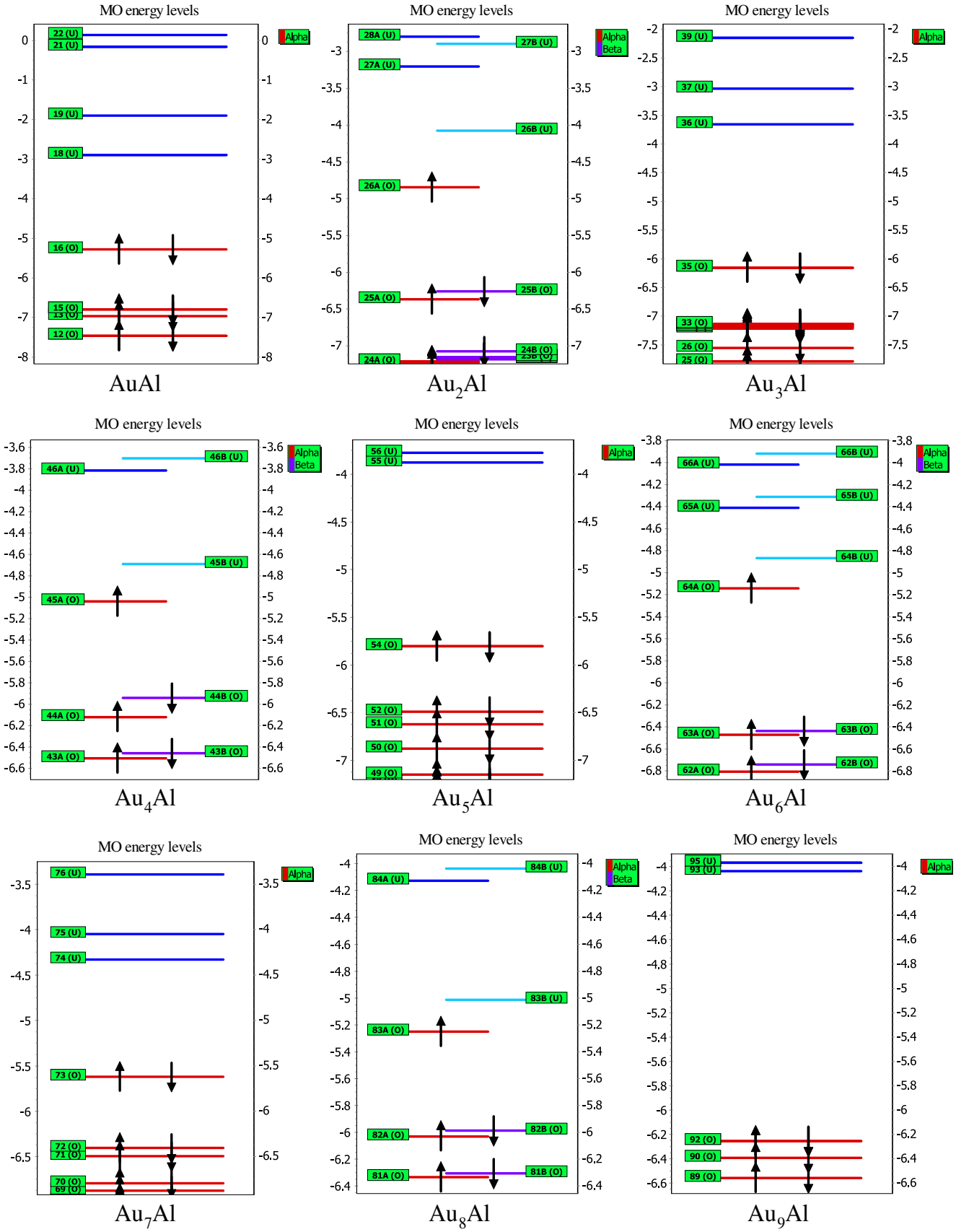
MO energy levels
Alpha
22 (U)
21 (U)
19 (U)
18 (U)
16 (O)
15 (O)
13 (U)
12 (O)
AuAl
MO energy levels
Alpha
Beta
28A (U)
27B (U)
27A (U)
26B (U)
26A (O)
25A (O)
25B (O)
24B (O)
24A (O)
Au2Al
MO energy levels
Alpha
39 (U)
37 (U)
36 (U)
35 (O)
33 (O)
26 (O)
25 (O)
Au3Al
MO energy levels
Alpha
Beta
46B (U)
46A (U)
45B (U)
45A (O)
44B (O)
44A (O)
43B (O)
43A (O)
Au4Al
MO energy levels
Alpha
56 (U)
55 (U)
54 (O)
52 (O)
51 (O)
50 (O)
49 (O)
Au5Al
MO energy levels
Alpha
Beta
66B (U)
66A (U)
65B (U)
65A (U)
64B (U)
64A (O)
63B (O)
63A (O)
62B (O)
62A (O)
Au6Al
MO energy levels
Alpha
76 (U)
75 (U)
74 (U)
73 (O)
72 (O)
71 (O)
70 (O)
69 (O)
Au7Al
MO energy levels
Alpha
Beta
84B (U)
84A (U)
83B (U)
83A (O)
82B (O)
82A (O)
81B (O)
81A (O)
Au8Al
MO energy levels
Alpha
95 (U)
93 (U)
92 (O)
90 (O)
89 (O)
Au9Al

eV, respectively, are located at the ground-state structures Au_3Al, Au_4Si, and Au_6. This result further confirms the dramatically enhanced chemical stabilities in these isomers.

Here, the electronic properties are also discussed by probing into the localization of Mulliken atomic charges within Au_nM (M = Al and Si) clusters. We can see that, for both ground-state Au_nAl and Au_nSi clusters, the charge values of M atoms are positive, while the values of Au in most cases are negative. This indicates that the charges in the corresponding isomer transfer from M atom to Au_n frame, which may come from a larger electronegativity of Au (2.54) than that of Al (1.61) and Si (1.90). Focusing on the gold atoms, it is found that their charge distribution is related to the symmetry of the cluster. Also, the calculated charges of impurity atoms exhibit a sequence of Au_nAl > Au_nSi, which is reversed in that of electronegativity.

Furthermore, aiming at understanding the internal charge transfer, the natural electron configurations (NEC) of gold and impurity atoms are taken into account on the basis of natural population analysis (results tabulated in Table 3). From Table 3, we find that 9.87-88.65 and 9.78-88.56 electrons, respectively, occupy the 5d subshells of the Au atoms in the lowest energy Au_nAl and Au_nSi clusters. The values reveal that the *d* orbitals of Au atoms in Au_nM (M = Al and Si) clusters can be viewed as dominant core orbital. With regard to impurities, the NEC values reveal that the 3 *s* states lose electrons 0.07-0.95, while the 3*p* states receive −0.48-1.21 electrons for Au_nAl clusters, and the 3*s* states lose 0.08-0.61 electrons, while the 3*p* states receive −0.20-1.04 electrons for Au_nSi clusters. The contribution of the 3*d* states is nearly zero, so it can be neglected. Guided by this, one can see that for $Au_{1,2,3,4,9}Al$ and $Au_{1,2,3,7}Si$ clusters, the electrons transfer from the impurity atoms to the Au atoms, and from the Au_n frame to the impurity atoms in the other clusters. Therefore, we conclude that the electronic charge distributions of Au_nM clusters are primarily governed by *s*- and *p*-orbital interactions, especially n=1–4. For Au-Si systems, which are accordant with the findings from VASP [18].

Magnetic properties

For the most stable structures, the total magnetic moment of Au_nM (M = Al and Si, n=1–9) and Au_{n+1} clusters are plotted in Fig. 6. There exhibits distinct odd-even alternations as a function of cluster size, that is, both doped and pure gold clusters where odd-number valence electrons have a total magnetic moment of $1\mu_B$. However, as shown in Fig. 5, for even ones where α and β spin orbitals are degenerate, their corresponding magnetic moments are zero. Also, due to the addition of one *p* electron, a reversed odd-even oscillation is found in Au-Si system. In order to further analyze the contributions of impurity and gold atoms to the total magnetic moments, the local magnetic moment of Al, Si, and Au atoms are listed in Table 4 and plotted in Fig. 6, respectively. It is shown that the local magnetic moments of impurity and gold atoms in the corresponding Au_nM (M = Al and Si) clusters exhibit a similar odd-even oscillatory, and for clusters with odd valence electrons, the local magnetic moments of impurity decrease drastically when *n* increases from 1 to 9 (except for Au_5Si). This indicates that the total magnetic moments of Au_nAl and Au_nSi clusters is mainly located on impurity atoms for Au_2Al and $Au_{1,3}Si$ clusters while on the gold atoms for $Au_{4,6,8}Al$ and $Au_{5,7,9}Si$ clusters. In Table 4, it is interesting to notice that the local magnetic moments of impurity atoms is mainly focused on *p* orbital, whereas the *s* orbital bring the biggest effect for gold atoms. Therefore, the magnetic properties of clusters are also related to a strong *s*-*p* orbital interaction.

Table 3 Natural electron configuration (NEC) of 3s, 3p, and 3d states for M atom and summated natural electron configuration (SNEC) of 6s, 5 d, and 6p states for Au atoms in the lowest energy Au_nM (M = Al and Si, n=1–9) and Au_n clusters at the PW91/GEN (6–311 G* for dopants and SDD for Au) level

Cluster size	Au_nAl		Au_nSi		Au_n
	NEC (Al)	SNEC (Au)	NEC (Si)	SNEC (Au)	SNEC (Au)
n=1	$3\,s^{1.93}3p^{0.52}3\,d^{0.01}$	$6\,s^{1.63}5\,d^{9.87}6p^{0.03}$	$3\,s^{1.92}3p^{1.81}3\,d^{0.01}$	$6\,s^{1.40}5\,d^{9.78}6p^{0.06}$	$6\,s^{1.00}5\,d^{10.00}6p^{0.00}$
n=2	$3\,s^{1.53}3p^{0.91}3\,d^{0.02}$	$6\,s^{2.72}5\,d^{19.74}6p^{0.06}$	$3\,s^{1.85}3p^{1.80}3\,d^{0.02}$	$6\,s^{2.62}5\,d^{19.58}6p^{0.12}$	$6\,s^{2.06}5\,d^{19.90}6p^{0.00}$
n=3	$3\,s^{1.26}3p^{1.31}3\,d^{0.03}$	$6\,s^{3.72}5\,d^{29.64}6p^{0.06}$	$3\,s^{1.60}3p^{2.36}3\,d^{0.03}$	$6\,s^{3.42}5\,d^{29.46}6p^{0.12}$	$6\,s^{3.21}5\,d^{29.67}6p^{0.12}$
n=4	$3\,s^{1.17}3p^{1.71}3\,d^{0.03}$	$6\,s^{4.36}5\,d^{39.44}6p^{0.28}$	$3\,s^{1.42}3p^{2.84}3\,d^{0.05}$	$6\,s^{4.12}5\,d^{39.36}6p^{0.20}$	$6\,s^{3.88}5\,d^{39.60}6p^{0.52}$
n=5	$3\,s^{1.08}3p^{2.14}3\,d^{0.03}$	$6\,s^{4.85}5\,d^{49.40}6p^{0.50}$	$3\,s^{1.49}3p^{2.87}3\,d^{0.05}$	$6\,s^{4.85}5\,d^{49.20}6p^{0.50}$	$6\,s^{4.85}5\,d^{49.45}6p^{0.70}$
n=6	$3\,s^{1.13}3p^{1.95}3\,d^{0.03}$	$6\,s^{5.88}5\,d^{59.22}6p^{0.84}$	$3\,s^{1.67}3p^{2.42}3\,d^{0.03}$	$6\,s^{5.64}5\,d^{59.04}6p^{1.14}$	$6\,s^{5.76}5\,d^{59.34}6p^{0.96}$
n=7	$3\,s^{1.06}3p^{2.21}3\,d^{0.03}$	$6\,s^{6.58}5\,d^{69.02}6p^{0.98}$	$3\,s^{1.65}3p^{2.31}3\,d^{0.02}$	$6\,s^{6.72}5\,d^{68.88}6p^{1.47}$	$6\,s^{6.65}5\,d^{69.16}6p^{1.19}$
n=8	$3\,s^{1.05}3p^{2.04}3\,d^{0.02}$	$6\,s^{7.76}5\,d^{78.80}6p^{1.28}$	$3\,s^{1.39}3p^{3.04}3\,d^{0.04}$	$6\,s^{7.36}5\,d^{78.80}6p^{1.28}$	$6\,s^{7.68}5\,d^{79.04}6p^{1.28}$
n=9	$3\,s^{1.07}3p^{1.28}3\,d^{0.02}$	$6\,s^{9.09}5\,d^{88.65}6p^{1.89}$	$3\,s^{1.39}3p^{3.00}3\,d^{0.04}$	$6\,s^{8.10}5\,d^{88.56}6p^{1.80}$	$6\,s^{8.28}5\,d^{88.83}6p^{1.89}$

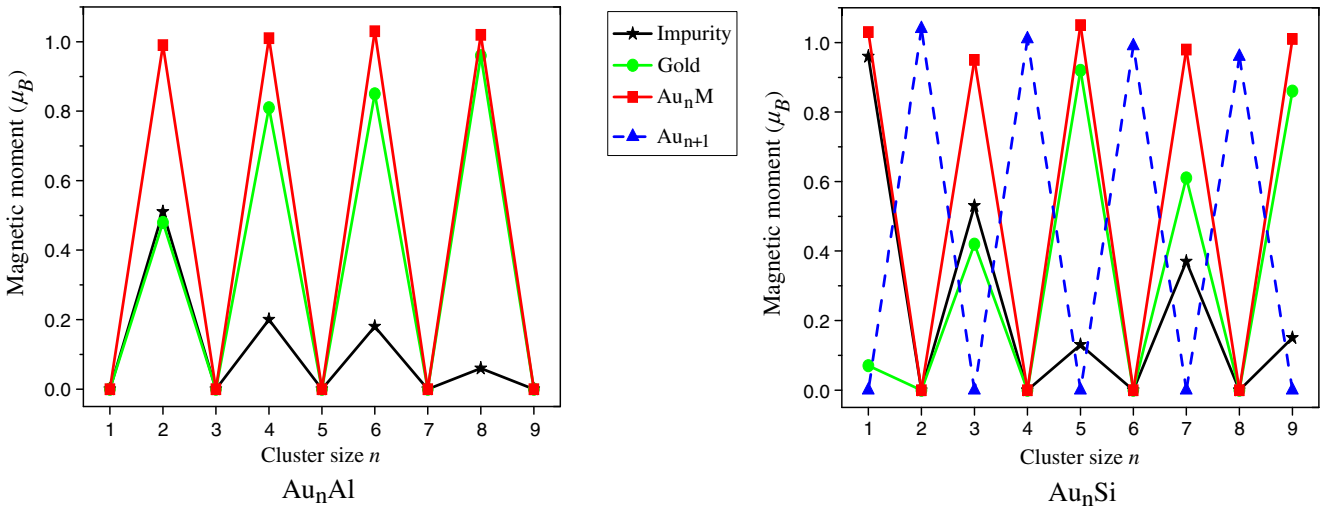

Fig. 6 Total magnetic moment for the lowest energy structures of Au_nM (M = Al and Si, n=1–9) and Au_{n+1} clusters, and local magnetic moment on M and gold atoms, respectively, in the corresponding Au_nM clusters at the PW91/GEN (6–311 G* for dopants and SDD for Au) level

Conclusions

Based on the first-principle method, we have presented a systematic study on geometrical structures, relative stabilities, electronic as well as magnetic properties of complexes Au_nM (M = Al and Si, n=1–9) and their comparisons with bare gold clusters. The main conclusions are made as follows.

(1) For the small sized Au_nM (M = Al and Si, n=1–9) clusters, aluminum or silicon substituted Au_{n+1} clusters and Au atom added Au_{n-1} M structures are two kinds of dominating growth patterns. Based on optimized stable configurations, we observe that the ground-state structures are 3D for n=4–8 in Au_nAl clusters and n=3–9 in Au_nSi clusters.

(2) The fragmentation energies, second-order difference of energies, and HOMO-LUMO energy gaps are studied as a function of cluster size in detail for each ground-state cluster. The calculated results show that there exhibit a similar odd-even alternative phenomenon, indicating that the magic numbers of stabilities are n=1, 3, 5, 7, 9 for Au_nAl and Au_{n+1} clusters, while n=2, 4, 6, 8 for Au_nSi clusters. In particular, we can conclude the clusters Au_3Al, Au_4Si, and Au_6 have a dramatically enhanced chemical stability due to the larger HOMO-LUMO energy gaps of 2.49, 2.06, and 2.16 eV, respectively. At the same time, the atomic

Table 4 Magnetic moment (μ_B) of 3s, 3p, and 3d states for M atoms and 6s, 5d, and 6p states for Au atoms, respectively, as well as the local magnetic moment on M and Au atoms in the lowest energy Au_nM (M = Al and Si, n=1–9) and Au_n clusters at the PW91/GEN (6–311 G* for dopants and SDD for Au) level

Cluster		Impurity/gold atoms								
		n=1	n=2	n=3	n=4	n=5	n=6	n=7	n=8	n=9
Au_nAl	3s/6s	0.00/0.00	0.28/0.44	0.00/0.00	0.03/0.63	0.00/0.00	0.05/0.58	0.00/0.00	0.00/0.64	0.00/0.00
	3p/6p	0.00/0.00	0.23/0.02	0.00/0.00	0.17/0.06	0.00/0.00	0.13/0.12	0.00/0.00	0.06/0.19	0.00/0.00
	3d/5d	0.00/0.00	0.00/0.02	0.00/0.00	0.00/0.12	0.00/0.00	0.00/0.15	0.00/0.00	0.00/0.13	0.00/0.00
	Sum	0.00/0.00	0.51/0.48	0.00/0.00	0.20/0.81	0.00/0.00	0.18/0.85	0.00/0.00	0.06/0.96	0.00/0.00
Au_nSi	3s/6s	0.00/0.02	0.00/0.00	0.15/0.36	0.00/0.00	0.13/0.73	0.00/0.00	0.03/0.33	0.00/0.00	0.13/0.60
	3p/6p	0.96/0.03	0.00/0.00	0.38/0.00	0.00/0.00	0.00/0.06	0.00/0.00	0.34/0.08	0.00/0.00	0.02/0.10
	3d/5d	0.00/0.02	0.00/0.00	0.00/0.06	0.00/0.00	0.00/0.13	0.00/0.00	0.00/0.20	0.00/0.00	0.00/0.16
	Sum	0.96/0.07	0.00/0.00	0.53/0.42	0.00/0.00	0.13/0.92	0.00/0.00	0.37/0.61	0.00/0.00	0.15/0.86
Au_{n+1}	6s	0.00	0.84	0.00	0.74	0.00	0.68	0.00	0.61	0.00
	6p	0.00	0.04	0.00	0.12	0.00	0.13	0.00	0.14	0.00
	5d	0.00	0.16	0.00	0.15	0.00	0.18	0.00	0.21	0.00
	Sum	0.00	1.04	0.00	1.01	0.00	0.99	0.00	0.96	0.00

average binding energies of doped gold clusters are higher than those of pure clusters.

(3) According to the calculated electronic structures, it is noticed that in the corresponding Au_nM (M = Al and Si, n=1–9) configurations M acts as an electron donor, and the charge transfer between *s* and *p* states contributes to the cluster properties. In addition, the odd-even alternative behaviors are found in the magnetic moment (total or local), for which the clusters with odd-number valence electrons show relatively larger magnetic effects. The inverse correlation of magnetic moment *vs* the fragmentation energy, second-order difference of energy, and HOMO-LUMO energy gap manifests that these clusters have lower magnetic moment, but higher stabilities. It is interesting that the magnetic properties of clusters are also related to a strong *s*-*p* orbital interaction.

Acknowledgments This work was supported by the Doctoral Education Fund of Education Ministry of China (No. 20100181110086) and the National Natural Science Foundation of China (No. 10974138 and 11104190).

References

1. Gupta K, Chanty TK, Chosh SK (2010) Phys Chem Chem Phys 12:2929–2934
2. Yamada T, Mawatari A, Tanabe M, Osakada K, Tanase T (2009) Angew Chem 121:576–579
3. Zappa F, Denifl S, Mähr I, Bacher A, Echt O, Märk TD, Scheier P (2008) J Am Chem Soc 130:5573–5578
4. Hempelmann F, Hölper S, Verhoefen MK, Woerner AC, Köhler T, Fiedler SA, Pfleger N, Wachtveitl J, Glaubitz C (2011) J Am Chem Soc 133:4645–4654
5. He H, Cao GJ, Zheng ST, Yang GY (2009) J Am Chem Soc 131:15588–15589
6. Lecoultre S, Rydlo A, Félix C, Buttet J, Gilb S, Harbich W (2011) J Chem Phys 134:074302
7. Häkkinen H (2008) Chem Soc Rev 37:1847–1859
8. Herzing AA, Kiely CJ, Carley AF, Landon P, Hutchings GJ (2008) Science 321:1331–1335
9. Baletto F, Ferrando R (2005) Rev Mod Phys 77:371–423
10. Lang SM, Bernhardt TM, Barnett RN, Yoon B, Landman U (2009) J Am Chem Soc 131:8939–8951
11. Alexandrova AN, Boldyrev AI, Li X, Sarkas HW, Hendricks JH, Arnold ST, Bowen KH (2011) J Chem Phys 134:044322
12. Gilb S, Weis P, Furche F, Ahlrichs R, Kappes M (2002) J Chem Phys 116:4094–4101
13. Häkkinen H, Yoon B, Landman U (2003) J Phys Chem A 107:6168–6175
14. Fernández EM, Soler JM, Garzón IL, Balbás LC (2004) Phys Rev B 70:165403
15. Lee HM, Ge M, Sahu BR, Tarakeshwar P, Kim KS (2003) J Phys Chem B 107:9994–10005
16. Li XB, Wang HY, Yang XD, Zhu ZH, Tang YJ (2007) J Chem Phys 126:084505
17. Deka A, Deka RC (2008) J Mol Struct (Theochem) 870:83–93
18. Majumder C (2007) Phys Rev B 75:235409
19. Yoon B, Häkkinen H, Landman U, Wörz AS, Antonietti JM, Abbet S, Judai K, Heiz U (2005) Science 307:403–407
20. Ghanty TK, Banerjee A, Chakrabarti A (2010) J Phys Chem C 114:20–27
21. Yuan DW, Gong XG, Wu RQ (2008) Phys Rev B 78:035441
22. Li X, Kiran B, Cui LF, Wang LS (2005) Phys Rev Lett 95:253401
23. Koszinowski K, Schröder D, Schwarz H (2003) ChemPhysChem 4:1233–1237
24. Joshi AM, Delgass WN, Thomson KT (2006) J Phys Chem B 110:23373–23387
25. Wang LM, Pal R, Huang W, Zeng XC, Wang LS (2010) J Chem Phys 132:114306
26. Wang HQ, Kuang XY, Li HF (2010) Phys Chem Chem Phys 12:5156–5165
27. Yuan DW, Wang Y, Zeng Z (2005) J Chem Phys 122:114310
28. Torres MB, Fernández EM, Balbás LC (2005) Phys Rev B 71:155412
29. Neukermans S, Janssens E, Tanaka H, Silverans RE, Lievens P (2003) Phys Rev Lett 90:033401
30. Chirawatkul P, Zeidler A, Salmon PS, Takeda S, Kawakita Y, Usuki T, Fische HE (2011) Phys Rev B 83:014203
31. Lee SH, Stephens JA, Hwang GS (2010) J Phys Chem C 114:3037–3041
32. Pal R, Wang LM, Huang W, Wang LS, Zeng XC (2009) J Am Chem Soc 131:3396–3404
33. Dailey E, Madras P, Drucker J (2010) J Appl Phys 108:064320
34. Ferralis N, Maboudian R, Carraro C (2008) J Am Chem Soc 130:2681–2685
35. Pal R, Cui LF, Bulusu S, Zhai HJ, Wang LS, Zeng XC (2008) J Chem Phys 128:024305
36. Choi YC, Lee HM, Kim WY, Kwon SK, Nautiyal T, Cheng DY, Vishwanathan K, Kim KS (2007) Phys Rev Lett 98:076101
37. Majumder C, Kandalam AK, Jena P (2006) Phys Rev B 74:205437
38. Li YF, Kuang XY, Wang SJ, Li Y, Zhao YR (2011) Phys Lett A 375:1877–1882
39. Li YF, Kuang XY, Wang SJ, Zhao YR (2010) J Phys Chem A 114:11691–11698
40. Frisch MJ et al (2004) GAUSSIAN 03 Revision E.01, Gaussian, Inc., Wallingford, CT
41. Perdew P, Chevary JA, Vosko SH, Jackson KA, Pederson MR, Singh DJ, Fiolhais C (1992) Phys Rev B 46:6671–6687
42. Dolg M, Wedig U, Stoll H, Preuss H (1987) J Chem Phys 86:866–872
43. Schwerdtfeger P, Dolg M, Schwarz WHE, Bowmaker GA, Boyd PDW (1989) J Chem Phys 91:1762–1774
44. Gingerich KA, Blue GD (1973) J Chem Phys 59:185–189
45. Cuthill AM, Fabian DJ, Shu-Shou-Shen S (1973) J Phys Chem 77:2008–2011
46. Scherer JJ, Paul JB, Collier CP, O'Keefe A, Saykally RJ (1995) J Chem Phys 103:9187–9192
47. Weast RC (ed) (1969) CRC Handbook of Chemistry and Physics, 49th edn. CRC, Cleveland, OH
48. Zhao LX, Feng XJ, Cao TT, Liang X, Luo YH (2009) Chin Phys B 18:2709–2718